Multi-asperity elliptical JKR model for adhesion of a surface with non-axially symmetric asperities

Stefano Perni [1,2] and Polina Prokopovich [1,2*]

[1]Cardiff School of Pharmacy and Pharmaceutical Science, Cardiff University, Cardiff, UK

[2]Department of Biological Engineering, Massachusetts Institute of Technology, Cambridge, MA, USA

Corresponding author: Dr Polina Prokopovich

School of Pharmacy and Pharmaceutical Science

Cardiff University

Redwood Building, King Edward VII Avenue

Cardiff, UK

CF10 3NB

E-mail address: prokopovichp@cf.ac.uk

Abstract

Surfaces can present high levels of topographic asymmetry and, therefore, theories based on the assumption of symmetry cannot be effectively employed.

A new multi-asperity adhesion model that assumes that asperities are not perfectly hemispherical is presented here, this model is based on the elliptical JKR model for a single asperity. The adhesion between a soft tissue with asperities greatly asymmetric and a polymer was modelled, the predicted adhesion forces were successfully validated against experimentally obtained data. Moreover, simulations with a simpler model, which assumes symmetrical asperities, have been also carried out; these results were significantly different from those obtained, using both the newly developed model and those determined experimentally. This highlights the importance of the model presented in this work.

Keywords: adhesion, JKR model, multi-asperity contact model, asymmetric asperities

1. Nomenclature

a, b Major and minor semi-axis of ellipse of contact

d Distance between two surfaces

e eccentricity of ellipse of contact

E reduced Young's modulus $E = \left(\frac{1-\upsilon_1^2}{E_1} + \frac{1-\upsilon_2^2}{E_2} \right)^{-1}$

E_x E_y Young modulii in orthogonal directions

E_1 E_2 Young modulii of contacting materials

$\boldsymbol{E}$(e) Complete elliptical integral of second kind $\boldsymbol{E}(\boldsymbol{e}) = \int_0^{\pi/2} \sqrt{1-e^2 \sin^2(\xi)}\, d\zeta$

F_{adh} Adhesion force

$fn\left(\delta_i, R_{\max,i}, R_{\min,i}\right)$ is the adhesion force for asperity i with curvature radii $R_{max,i}$ and $R_{min,i}$ and deformation δ_i based on the elliptical JKR model for a single asperity

h_i Height of asperity i

$\boldsymbol{K}$(e) Complete elliptical integral of first kind $\boldsymbol{K}(\boldsymbol{e}) = \int_0^{\pi/2} \frac{d\zeta}{\sqrt{1-e^2 \sin^2(\xi)}}$

p Shape parameter of Weibull distribution

$P_0 = \frac{Ea^2}{2bRe} \frac{\alpha' - \beta' \left(\frac{b}{a}\right)^{5/2}}{1-\left(\frac{b}{a}\right)^{1/2}}$ Contact pressure in the centre of the ellipse

$R_{max,i}$ $R_{min,i}$ Principal curvature radii of asperity i

$Re = \sqrt{R_{\max} R_{\min}}$

W Applied load of a single asperity

$$\alpha' = \frac{2bRe}{E}\alpha$$

$$\beta' = \frac{2bRe}{E}\beta$$

$\Delta\gamma = \gamma_1^{TOT} + \gamma_2^{TOT}$ Sum of surface energies of contacting materials

δ_i Deflection of asperity i

$\delta_{c.i}$ Critical deflection of asperity i with curvature radii $R_{max,i}$ and $R_{min,i}$

ε Scale parameter of Weibull distribution

γ^{AB} Acid-base component of the surface free energy

γ^{LW} Apolar component of the surface free energy

γ^{TOT} Total surface energy

γ^{-} Electron-donor component of the acid-base surface free energy

γ^{+} Electron-acceptor component of the acid-base surface free energy

$\lambda = \sqrt{\frac{R_{\min}}{R_{\max}}}$

ν_1, ν_2 Poisson ratios of contacting materials

Φ Cumulative distribution function

2. Introduction

Adhesion is very important in many circumstances, for example in pharmaceutical formulations, [1] biofilm formation, [2] insects climbing, [3] particles interaction [4] and wear and frictional performance of materials. [5]-[8] Because of the detrimental or required effect of adhesion, depending on the circumstances, the ability of predicting such phenomena is very helpful in technology developments. [1][1],[5] Every material exhibits surfaces that present geometrical irregularities, this generally random phenomena is known as surface roughness and is a critical aspect of adhesion [8] and other functional properties. [9],[10]

Numerous theories have been proposed to describe the adhesion phenomena between surfaces; some are single asperity based, [11][11]-[15][15] whilst others consider a multi-

Formatted: English (U.K.)

Formatted: English (U.K.)

Formatted: English (U.K.)

asperities contact situation. [16][16]-[19][19] Generally, multi-asperity adhesion models starts from theories describing the interaction between a single sphere/particle or asperities to a flat surface [20][20],[21][21] and integrate the overall interaction between rough surfaces considering the distributions of the asperities geometrical properties such as height and curvature radii. [19][19]-[24][24] Commonly, surface asperities are assumed to have a perfectly symmetrical top (so called perfectly hemi-spherically tipped); this is because many materials present surface asperities with a minimal degree of asymmetry. [25][25] Multi-asperity adhesion models, which assume perfectly hemispherically-tipped asperities, can still be used when this assumption is not verified providing that the geometrical average of the radii of curvature in orthogonal directions is used. [25][25] The distribution of the parameters representing the surface roughness are dependent on the manufacturing process and, despite, often following a Gaussian profile, this theory does not cover all type of surfaces; some materials are machined in such a way that their surface presents highly asymmetric asperities such as grooves. [26][26],[27][27]

Recently, Prokopovich and Perni have developed a series of adhesion models [19][19],[5][5],[28][28] where, progressively, limiting assumptions were removed. In this paper, a new multi-asperity adhesion model, based on the elliptical JKR model for a single asperity, is presented and applied to the contact between a soft tissue (urethra tissue) and a PVC (polyvinylchloride) material. The elliptical JKR theory, removes the assumption that the asperities are, even mildly, hemispherically tipped; therefore, it is appropriate for surfaces that show a very high level of asymmetry of the radii of curvature for their asperities. In this work, the adhesion forces between the surface of urethra (here used a model surface for materials presenting surfaces with non-hemispherically tipped asperities) and PVC was modelled, taking into account the effects of a large number of asperities on the surfaces. Surface energy, elastic moduli and surface asperity properties (height and radii of curvature)

Formatted: English (U.K.)
Formatted: English (U.K.)
Formatted: English (U.K.)
Formatted: English (U.K.)
Formatted: English (U.K.)
Formatted: English (U.K.)
Formatted: English (U.K.)
Formatted: English (U.K.)
Formatted: English (U.K.)
Formatted: English (U.K.)
Formatted: English (U.K.)
Formatted: English (U.K.)
Formatted: English (U.K.)

were determined for urethra tissue. These predictions were successfully compared with experimental data.

3. Theory

3.1. Adhesive contact for an asperity with different radii of curvature (elliptical JKR model)

Johnson and Greenwood [29][~~29~~] presented the solution of the JKR model for the contact between an asperity, with two different radii of curvature in orthogonal directions (R_{max} and R_{min}), and a perfectly flat surface. However, their solution starts from the preliminary knowledge of the ratio between the two semi-axes of the ellipse of contact (b/a). The individual values for the semi-axes of the ellipse of contact and the contact pressure can be calculated from this asperity deformation data. Furthermore, unlike the Hertz theory, R_{max} / R_{min} does not determine b/a univocally as the shape of the ellipse of contact varies with asperity deformation.

Formatted: English (U.K.)

The following parameters are used to characterise the asperity and the contact area:

$$\lambda = \sqrt{\frac{R_{min}}{R_{max}}} \qquad Re = \sqrt{R_{max}R_{min}} \qquad e^2 = 1-\left(\frac{b}{a}\right)^2 \tag{1}$$

The complete elliptical integrals, of first and second kind, $\boldsymbol{K}(e)$ and $\boldsymbol{E}(e)$ are estimated and the coefficients of the following matrix are calculated, then the corresponding system can be solved:

$$\begin{bmatrix} C(e) + D(e) & -\left(\frac{b}{a}\right)^2 C(e) \\ -C(e) & B(e) + \left(\frac{b}{a}\right)^2 C(e) \end{bmatrix} \begin{bmatrix} \alpha' \\ \beta' \end{bmatrix} = \begin{bmatrix} \lambda \\ 1/\lambda \end{bmatrix} \tag{2}$$

Where:

$$e^2\boldsymbol{D}(e) = \boldsymbol{K}(e) - \boldsymbol{E}(e) \qquad \boldsymbol{B}(e) = \boldsymbol{K}(e) - \boldsymbol{D}(e) \qquad e^2\boldsymbol{C}(e) = \boldsymbol{D}(e) - \boldsymbol{B}(e)$$

The semi-axes of the ellipse of contact are calculated, once the unit-less coefficients α' and β' have been estimated, (until this stage has been completed, only the ratio between the two semi-axes is known) as:

$$a^{3/2} = 2Re\sqrt{\frac{2\Delta\gamma}{\pi E}}\frac{\left(\frac{b}{a}\right)^{1/2}\left(1-\left(\frac{b}{a}\right)^{1/2}\right)}{\beta'\left(\frac{b}{a}\right)^{2}-\alpha'} \tag{3}$$

And subsequently:

$$b = a\left(\frac{b}{a}\right) \quad \Rightarrow \quad b(e) \tag{4}$$

The contact pressure in the centre of the ellipse is:

$$P_0 = \frac{Ea^2}{2bRe}\frac{\alpha'-\beta'\left(\frac{b}{a}\right)^{5/2}}{1-\left(\frac{b}{a}\right)^{1/2}} \tag{5}$$

The asperity deformation determined as:

$$\delta = \left(\frac{b}{E}\right)\left[2P_0\boldsymbol{K}(e) - \frac{\alpha' E}{2bRe}a^2\boldsymbol{B}(e) - \frac{\beta' E}{2bRe}b^2\boldsymbol{B}(e)\right] \quad \Rightarrow \quad b(\delta) \tag{6}$$

In our model, the deformation δ is known instead of the ratio *b/a* as in the original formulation of the elliptic JKR model for one asperity. Therefore, an iterating process was adopted. For a known deformation, δ, the ratio *b/a* is assumed and the system in Equ. 2 is solved. A value of *b*, denoted *b(e)*, is obtained from the solutions α' and β' and Equ. 3 and 4. Then, using the known value of the deformation δ and Equ. 6, another value of *b* is obtained, this is denoted *b(δ)*. The values of *b(e)* and *b(δ)* are compared and, if the difference is greater than a set accepted error, a new ratio *b/a* is assumed and the process repeated until convergence. The algorithm used is shown in Figure 1~~Figure 1~~. The error between the two calculated values of *b*(δ) and *b(e)* was set to be less than 1%.

Finally, the area of contact calculated:

$$\mathrm{A_{cont}} = \pi ab \tag{7}$$

And the applied load is calculated according to the following equation:

$$W = 2\pi ab\left[P_0 - \frac{1}{3}(\alpha a^2 + \beta b^2)\right] \quad (8)$$

3.2. Adhesive contact between surfaces (multi-asperity adhesion model)

The proposed model, which estimates the contact force between one perfectly flat surface and one which presents non-hemispherical asperities, is presented in Figure 2~~Figure 2~~. In our case, the PVC is assumed to be flat and the urethra is assumed to be rough, as the roughness of PVC material is significantly lower than that of the urethra. The first stage of this process is the generation of a set of asperities (10,000) with varying heights and curvature radii, using the Monte Carlo method and experimentally obtained distributions of these parameters.

The second stage of the simulation is the calculation of the total contact force F_{adh} as a function of the separation distance (d) using the elliptical JKR model for a single asperity. The overall contact force ($F_{adh}(d)$) is calculated as the sum of all individual contact forces, generated by the asperities whose heights (h_i) exceed d or are within a critical distance $\delta_{c,i}$. [19]~~[19]~~,[5]~~[5]~~,[28]~~[28]~~,[30]~~[30]~~:

$$F_{adh}(d) = \sum_{i}^{\delta_i > -\delta_{c,i}} fn\left(\delta_i, R_{\max,i}, R_{\min,i}\right) \quad (9)$$

Where:

$$\delta_i = h_i - d \quad (10)$$

$fn\left(\delta_i, R_{\max,i}, R_{\min,i}\right)$ is the adhesion force for asperity i with curvature radii $R_{max,i}$ and $R_{min,i}$ and deformation δ_i based on the elliptical JKR model for a single asperity and obtained as described above. The critical deformation of a non-hemispherically tipped asperity was calculated from the definition for the original JKR theory [29]~~[29]~~ and taking into account its dependence on R_{max} / R_{min} (Figure A1):

Formatted: English (U.K.)
Formatted: English (U.K.)
Formatted: English (U.K.)
Formatted: English (U.K.)
Formatted: English (U.K.)

$$\delta_{c,i} = K_c(Re_i)\left[3*\left(\frac{3}{2}\right)^{-2/3}\frac{\left(\frac{9\pi Re_i^{\,2}\Delta\gamma}{4E}\right)^{2/3}}{Re_i}\right] \quad (11)$$

Kc was calculated from fitting the simulated data (Figure A2) as:

$$(1 - K_c) = 0.0437x^2 + 0.0827x \quad (12)$$

where x = $\log_{10}(R_{max} / R_{min})$

Finally the calculated adhesion force was divided by the area correspondent to the number of asperities simulated to obtained the adhesion pressure. Simulations were repeated with 50 times independent sets of asperities to evaluate the distribution of the adhesion forces predicted.

4. Materials and Methods

4.1. Materials

The urethra tissues of commercial male pigs were obtained from a local abattoir. The samples were placed in PBS solution and stored at 4 °C during transport. Immediately after arrival in the laboratory, urethra tissue was carefully dissected and subsequently analysed without delay.

Rüsch Simplastic PVC material (Rüsch UK Ltd., UK) were used in this study.

4.2. Contact angle measurements and Surface energy determination

Pieces of urethra, approximately 1x1 cm, were cut, placed on a microscope glass-slide and left to dry at 37 °C until the contact angle of water was constant (about 30 minutes). Three probe liquids of different polarities were used: distilled water, ethylene glycol and hexadecane (Sigma Aldrich, UK). Images of a liquid drop of 5 µl volume, deposited on the urethra surface, were taken immediately after deposition. Contact angles, at both the right and

the left side, were measured using ImageJ software (National Institutes of Health, USA http://rsbweb.nih.gov/ij/). Contact angles, obtained from 10 individual urethra samples, were calculated for each liquid. This was performed on samples taken from three different animal specimens.

The surface energy of a material (γ^{TOT}) comprises of four components: the apolar contribution associated with Lifshitz-Van der Waals interactions (γ^{LW}) and the acid-base component of surface free energy (γ^{AB}). The acid-base term is further expressed in term of the electron-donor (γ^{-}) and electron-acceptor (γ^{+}) parameters.

$$\gamma^{AB} = 2\sqrt{\gamma^{+}\gamma^{-}} \tag{13}$$

The relationship between the contact angle of a liquid on a surface and the surface energy components of both the surface and the liquid is: [32]~~[32]~~

Formatted: English (U.K.)

$$\cos\theta_L^S = \frac{2}{\gamma_L^{TOT}}\left(\sqrt{\gamma_S^{LW}\gamma_L^{LW}} + \sqrt{\gamma_S^{+}\gamma_L^{-}} + \sqrt{\gamma_S^{-}\gamma_L^{+}}\right) - 1 \tag{14}$$

The determination of the contact angles of three liquids of known properties and the solution of the system is usually employed to estimate the surface energy parameter of a material. When Equ. 14 is written for all the three liquids a system containing the three variables (surface properties of the materials) is obtained and the remaining four quantities for each liquid are known.

4.3. Surface topography

Urethra tissue surface coordinates were obtained using a Talysurf CLI 2000 scanner on an area with a size of 50 x 50 µm and at 50 µm/sec scan speed. The spacing along the x axis and y axis was equal to 0.5 µm. Three independent samples were scanned. Asperities were located setting the conditions proposed by [19]~~[19]~~. This is expressed mathematically as:

Formatted: English (U.K.)

$$z(i,j) \in asperities \Leftrightarrow z(i,j) > z(m,n) \quad \text{with} \quad m \quad \text{and} \quad n = i-2, i-1, i, i+1, i+2 \quad and \quad m,n \neq i,j$$

After the asperities were located, their heights were determined against a reference plane set as the average of all surface coordinates. The asperity height cumulative distribution was determined and fitted to the Gaussian model. The density of asperities was determined by calculating the number of observed asperities in the scanned area.

The principal asperity curvature radii (R_{max} and R_{min}) were determined by fitting the 25 coordinates of the points bordering the asperity with the following parabolid equation using the minimal residual squares approach (Figure 3~~Figure 3~~):

$$z = Ax^2 + By^2 + Cx + Dy + Fxy + G \tag{15}$$

The eigenvalues (k_1 and k_2) of the corresponding Hessian matrix were calculated as:

$$k_1 = (\mathrm{A}+\mathrm{B}) + \sqrt{(\mathrm{A}-\mathrm{B})^2 + F^2} \qquad k_2 = (\mathrm{A}+\mathrm{B}) - \sqrt{(\mathrm{A}-\mathrm{B})^2 + F^2} \tag{16a,b}$$

$$\text{And } R_{max} = -\frac{1}{\min(k_1, k_2)} \text{ and } R_{min} = -\frac{1}{\max(k_1, k_2)} \tag{17a,b}$$

The cumulative distributions for asperity curvature radii were obtained and fitted with both the Gaussian (Equ. 18) and Weibull model (Equ. 19).

$$\Phi(R) = \frac{1}{\sigma\sqrt{2\pi}} \int_{-\infty}^{R} \exp\left(-\frac{(\mu-\xi)^2}{2\sigma^2}\right) d\xi \tag{18}$$

$$\Phi(R) = 1 - \exp\left(-\frac{R}{\varepsilon}\right)^p \tag{19}$$

The direction of the principal radii of curvature could be determined as the eigenvectors of the Hessian matrix of Equ. 15.

4.4. Stress-strain analysis

The Young's modulus of the urethra samples was determined by performing uniaxial stress-strain analysis in orthogonal directions with an Instron 3366 (10 kN capacity) using the mechanical wedge action grips. Samples were prepared as described above. Sections 1 x 6

mm thick, were stretched at a speed of 35 mm/min, from an initial distance between the grips of 30 mm; 5 individual specimens were analysed.

4.5. Experimental measurement of adhesion force

The adhesion force between urethra and PVC was measured employing a texture analyser (TA.XT plus and a load cell equal to 30 kg) using the tensile grips (A/TG); the protocol was previously described. [33]~~[33]~~ Adhesion force has been determined as the maximum detachment force from the force-elongation curve. At least six replicates were obtained to determine the average adhesion force presented here for each case.

Formatted: English (U.K.)

4.6. Data fitting

Experimentally obtained cumulative distributions of asperity height and curvature radii were fitted with both Gaussian and Weibull distributions. The fitting parameters were determined using SigmaPlot (ver. 12.0) and Residual Sum of Squares (RSS) were estimated and used to assess the order of "best fit" of the model.

5. Results

5.1. Surface properties of urethra

Total surface energy of urethra is predominantly due to the van der Waals contribution (γ^{LW}). Water (57.0 °±2.8) has the highest contact angle, whilst hexadecane has the lowest contact angle of the three liquids studied (Table 1~~Table 1~~).

The cumulative distribution of the asperity height and the fitting with a Gaussian model are shown in Figure 4~~Figure 4~~. It is evident, that this statistical distribution describes the experimental data well. Urethra tissue had $6.24 \cdot 10^{10}$ asperities per m^2 with an average height of 4.37 μm and a standard deviation of 3.32 μm (Table A1). The actual value of asperity height is due to the choice of the reference plane. A negative value for this parameters means

that the asperity top is below the average of all the surface coordinates (the choice as reference plane in this work). The condition set to identify asperity on the surface using 25 points instead of the simpler 9 point was made because of the fitting of the asperity surface with a paraboloid containing 6 coefficients would not have been carried out on a sufficient number of experimental data. The high density of points on the surface was used to compensate the possible risk of missing actual asperities.

The assumption that asperity tips are perfectly hemispherical was tested in Figure 5~~Figure 5~~, where the frequency of the ratio between the two radii is presented. The highest occurrence was at a ratio of around 18 and some asperities had a ratio R_{max}/R_{min} greater than 100. This illustrates that the asperities are far from being hemispherical and the elliptical approximation of asperity shape is the most suitable for modelling the adhesion of urethra. No correlation was found between R_{max} and R_{min} (coefficient of correlation = 0.13); additionally, both principal radii of curvature were independent from the asperity height as the coefficient of correlations were 0.20 for R_{max} and 0.07 for R_{min} respectively (Figure A4 and A5).

This was also evident in the 3D image of the surface of urethra (Figure A2) that clearly revealed how asperities on the surface were stretched along one axis and aligned in a pattern resulting in grooves. Histological images of urethra appeared to reveal the same type of surface structure. [34]~~[34]~~

Formatted: English (U.K.)

The cumulative distribution of radii of curvature of the asperities, along with their respective fitting parameters for both Gaussian and Weibull models, are presented in Figure 6~~Figure 6~~. Both R_{max} and R_{min} were not well represented by a Gaussian model, being better described by the Weibull distribution. This was also confirmed by the value of the Residual Sum of Squares (RSS) which was almost an order of magnitude lower in case of the Weibull model than the Gaussian model for both the R_{max} and the R_{min} (Table A2).

The values of Young moduli in orthogonal directions (107 ± 14 and 82 ± 12 KPa) are not identical but similar demonstrating a small degree of anisotropy of the urethra tissue.

5.2. Estimation of contact force and real area of contact

The surface and material properties of PVC, used in the model presented here, were taken from Prokopovich and Perni [5]~~[5]~~, where such properties, were measured on the same type of PVC material.

An example of the predicted profile of the contact force against the separation distance is presented in Figure 7~~Figure 7~~a. The contact force between two contacting materials decrease to a minimum (referred to as "adhesive force") with increasing relative separation from an initial very close proximity; when the separation distance is increased further the contact force increases monotonically to zero when the two surfaces are far apart. [19]~~[19]~~,[5]~~[5]~~,[28]~~[28]~~ Negative values of contact force mean attraction and positive values mean that a force has to be applied. The profile obtained here, and shown in Figure 7~~Figure 7~~a, was consistent with those found in many other works. [19]~~[19]~~,[5]~~[5]~~,[28]~~[28]~~,[35]~~[35]~~ The corresponding relationship between contact force and real area of contact is reported in Figure 7~~Figure 7~~b and shows a monotonic increase in contact area with increasing applied load, however this relation is not linear, particularly at small values of applied loads.

The distribution of the adhesive force predicted from independent sets of asperities is shown in Figure 8~~Figure 8~~, the average value was 74 ± 14 N/m^2; this was very close with the results of the experimental measurements of adhesive pressure between urethra and PVC that were 65 ± 9 N/m^2.

Formatted: English (U.K.)

Formatted: English (U.K.)

Formatted: English (U.K.)

Formatted: English (U.K.)

Formatted: English (U.K.)

Formatted: English (U.K.)

Formatted: English (U.K.)

Formatted: English (U.K.), Check spelling and grammar

5.3. Comparison between the elliptical JKR model and the simplified adhesion model, using geometrical average of radii of curvature

Simulations were carried out with simplification of the geometrical average of the curvature radii and shown in Figure 7~~Figure 7~~, to determine how the predictions, using the new proposed model, compare to those that utilises such approximation.[25]~~[25]~~ Both the profiles for contact force and the real area of contact follow the same pattern. However, importantly, the values are different from those obtained with the new model based on the elliptical JKR theory; the adhesion forces are predicted to be 330 N/m^2 instead of 74 N/m^2.

Formatted: English (U.K.)

The elliptical JKR theory for a single asperity, predicts that, as the deformations increase, the profiles for contact area tends to the Hertzian shape. Therefore, the discrepancy between the use of a multi-asperity adhesion model, based on hemispherically tipped asperities, and the one presented in this work, which is not restricted to such a condition, increases at high values of deformation.

6. Discussion

The tissue structure of urethra is characterised by the presence of transitional epithelium (urethelium), and one of the main functions of this tissue is to act as barrier between urine and the rest of the body. Another function is the ability to stretch in order to cope with contraction and dilatation cycles. This feature is achieved through the high concentration of connective tissue, such as collagen. [36]~~[36]~~ Vena cava is also rich in collagen [37] and, therefore, the similarity of contact angles, and consequent surface energy parameters, between urethra and vena cava can be attributed to the high presence of collagen in both tissues. [5]~~[5]~~ However, for urethra, the contact angle of water is equal to 57° (Table 1~~Table 1~~) which is lower than the contact angle of water on aorta tissue (88°). Moreover, a Gaussian

Formatted: English (U.K.)

Formatted: English (U.K.)

distribution of asperity heights was obtained also for other biological tissues, such as: aorta and vena cava. [5]~~[5]~~

Anisotropy of native tissues varies, depending on locations and pathological conditions. [38]~~[38]~~ Recently, several researchers studied anisotropic properties of biological tissues, using different methods, such as stress-strain analysis [39]~~[39]~~ and nanoindentation. [40]~~[40]~~ Korossis *et al.* [39]~~[39]~~ reported a major regional and directional anisotropy in the quasi-static, uniaxial mechanical properties of the passive urinary bladder. Lillie *et al.* [41]~~[41]~~ studied uniaxial and biaxial mechanical properties of purified elastic tissue from the proximal thoracic aorta to understand physiological load distributions within the arterial wall. Sokolis [42]~~[42]~~ observed topographical variations and anisotropy in material parameters of porcine tissues (arteries) followed by relevant variations in histomorphometrical results. For the simulation a single value of Young modulus (the average of the two) was used because the two are very close. It has been shown that anisotropic mechanical properties determine a directional effect of the force of adhesion only when the values of elasticity in the principal directions differ for at least a few orders of magnitude. [43]~~[43]~~In the current model, the two principal radii of curvatures are independently simulated, furthermore, they were not correlated as analysis of these characteristics were found not be linked. However, it is possible to alter this part of the simulation, when this hypothesis is not found to be true, through using the generated asperity height to generate both principal radii of curvature.

In general, multiasperity adhesion models assume that asperities are symmetrical and, therefore, each asperity is described by its own single value of radius of curvature. [5]~~[5]~~,[17]~~[17]~~,[19]~~[19]~~,[28]~~[28]~~. Greenwood's [25]~~[25]~~ proposal of using models which assume perfectly hemispherical asperities with a radius of curvature equivalent to the geometrical average of *Rmax* and *Rmin*, is valid only if the ratio between the two is no more than about 10. [25]~~[25]~~ In urethra case, this is not possible as the ratio between radii is greater

Formatted: English (U.K.)
Formatted: English (U.K.)
Formatted: English (U.K.)
Formatted: English (U.K.)
Formatted: English (U.K.)
Formatted: English (U.K.)
Formatted: English (U.K.)
Formatted: English (U.K.)
Formatted: English (U.K.)
Formatted: English (U.K.)
Formatted: English (U.K.)

than 10. This is also shown by the different results obtained when this assumption was implemented instead of the full elliptical JKR model (Figure 7~~Figure 7~~). This confirms the need for a new model to be adopted; moreover, the almost-disappearance of the nose of the area of contact curve using the full ellipsoidal model could be attributed to the lower forces estimated at corresponding deformation than using the simplified geometrical average. The lower forces are a consequence of the shorter critical distance, resulting in asperity stretching, when the elliptical model is employed compared to the geometrical average approximation.

Numerous studies have reported that the adhesion force between two surfaces is not a single value but is described by a distribution of values as also found in this work. [19]~~[19]~~,[45]~~[45]~~,[46]~~[46]~~ This has been attributed to the fact that the properties of the asperities in the contact area (heights and curvature radii) can vary from one point on the surface to another, particularly, when the adhesion occurs between small contact areas (in the order of μm^2) containing a few asperities. The resulting adhesion force had different values as a consequence, this phenomenon was taken into account in our model through repeating the simulation with numerous sets of independently generated asperities. The real area of contact increases monotonically from zero with a typical profile. [28]~~[28]~~,[47]~~[47]~~ It can not be assumed to be linear along the full range of contact force, but only in restricted intervals and at high values of contact force.

The assumption that contact is only between a few independent asperity is a simplification valid for small applied loads, when these are high the contact will involve not only asperities and therefore other approaches are needed. The model proposed here, can be applied to the contact of materials with asperities which present the highest degree of asymmetry and when the adhesive contribution to the contact force can not be neglected as long as the material does not present a great level of mechanical anisotropy. This situation seems to match very closely the contact involving not only biological tissues, but also materials presenting

Formatted: English (U.K.)
Formatted: English (U.K.)
Formatted: English (U.K.)
Formatted: English (U.K.)
Formatted: English (U.K.)

grooves on the surfaces, consequence of machining processes such as: turning and milling. [48][~~48~~] Recently, also the surface of spinal discs utilised in Total Disc Replacement operation have been shown to display a surface characterised by spiral grooves originating from the top of disc dome. [49][~~49~~] Furthermore, the use of the normal distribution to describe the asperity heights was a consequence of the experimental data obtained as the use of the Weibull theory for the curvature radii.. As the Monte Carlo method is employed in order to generate the set of asperities used in the calculation, any other statistical distribution can be implemented, if found to better describe either asperity heights or curvature radii. [50][~~50~~]-[54][~~54~~]

Formatted: English (U.K.)

Formatted: English (U.K.)

Formatted: English (U.K.)

Formatted: English (U.K.)

7. Conclusion

The JKR model, for the elliptical contact of a single not hemispherical asperity, has been employed and integrated into a new multi-asperity adhesion model. This model is capable of predicting the profile of the contact force and real area of contact between two materials. It has been used to predict the adhesion between urethra (a model for surfaces with not axial-symmetric asperities) and PVC material. In order to do this, asperity height and curvature radii distributions, along with surface energy of urethra, were measured and presented for the first time.

The model proposed here can be applied to any material that presents non-symmetrical asperities, not just urethra. For example, some machining processes can result in grooves present on surfaces. Such features cannot be assumed to be perfectly hemispherical. Therefore, such contact can only be fully described with the model proposed here.

References

[1] E.C. Preedy, S. Perni, P. Prokopovich, Rev. Adhesion Adhesives 22 (2014) 226-252.

[2] E.C. Preedy, S. Perni, D. Nipiĉ, K. Bohinc, P. Prokopovich, Langmuir30(31) (2014) 9466-9476.

[3] Y. Zhou, A. Robinson, U. Steiner, W. Federle, Insect adhesion on rough surfaces: analysis of adhesive contact of smooth and hairy pads on transparent microstructured substrates. J. Royal Soc. Interface 11(98) (2014) 20140499.

[4] W. Sun, Q. Zeng, A. Yu, Calculation of noncontact forces between silica nanospheres. Langmuir 29(7) (2013) 2175-2184.

[5] P. Prokopovich, S. Perni, Frictional Behaviour Prediction of Mammalian Tissue Against Biomaterials. Acta Biomat. 6 (2010) 4052-4059

[6] B. Bhushan, Introduction to Tribology, Wiley, New York, 2002.

[7] B. Bhushan, Handbook of Micro/Nanotribology, CRC press, Boca Raton, FL, 1999.

[8] B. Bhushan, Contact mechanics of rough surfaces in tribology: multiple asperity contact. Tribology Lett. 4 (1998) 1-35.

[9] H.P. Papanagiotou, S.M. Morgano, R.A. Giordano, R. Pober, In vitro evaluation of low-temperature aging effects and finishing procedures on the flexural strength and structural stability of Y-TZP dental ceramics. J. Prosthet. Dent. 93 (2006) 154-164.

[10] N. De Jager, A.J. Feilzer, C.L. Davidson, The influence of surface roughness on porcelain strength. Dental Mater. 16 (2000) 381-388.

[11] K.L. Johnson, K. Kendall, A.D. Roberts, Surface energy and the contact of elastic solids. Proc. Royal Soc. London Ser. A 324(1558) (1971) 301-302.

Formatted: English (U.S.)

Formatted: English (U.S.)

[12] S.M. You, M.P. Wan, Modeling and Experiments of the Adhesion Force Distribution between Particles and a Surface. Langmuir 30(23) (2014) 6808-6818.

[13] B.V. Derjaguin, V.M. Muller, Y.P. Toporov, Effect of Contact Deformations on Adhesion of Particles. J. Colloid Interface Sci. 53(2) (1975) 314-326.

[14] D. Maugis, Adhesion of spheres: The JKR– DMT transition using a Dugdale model. J. Colloid Interface Sci. 150 (1992) 243-269.

[15] B. Bhushan, Contact mechanics of rough surfaces in tribology: single asperity contact. ASME J. Appl. Mech. Rev. 49 (1996) 275-298.

[16] J.F. Archard, Elastic Deformation and the Laws of Friction. Proc. Royal. Soc. A 243 (1957) 190-205.

[17] J.A. Greenwood, J.P.B. Williamson, Contact of nominally flat surfaces. Proc. Royal Soc. London Ser. A A295 (1966) 300-319.

[18] A.W. Bush, R.D. Gibson, T.R. Thomas, The elastic contact of a rough surface. Wear 35 (1975) 87-111.

[19] P. Prokopovich, S. Perni, A Multi-asperity Contact Adhesion Model for Universal Asperity Height and Radius of Curvature Distributions. Langmuir 26(22) (2010) 17028-17036.

[20] S. You, M.P. Wan, Mathematical models for the van der Waals force and capillary force between a rough particle and surface. Langmuir 29 (2013) 9104-9117.

[21] P. Prokopovich, V. Starov, Adhesion models: from single to multiple asperity contacts. Adv. Colloid Interface Sci. 168(1-2) (2011) 210-222.

[22] C.A. Kotwal, B. Bhushan, Contact analysis of non-Gaussian surfaces for minimum static and kinetic friction and wear. STLE Tribol. Trans. 39 (1996) 890-898.

[23] A.A. Polycarpou, I. Etsion, Analytical approximations in modelling contacting rough surfaces. ASME J. Tribol., 121 (1998) 234-239.

[24] G. Liu, Q.J. Wang, C. Lin, A survey of current models for simulating the contact between rough surfaces. STLE Tribol. Trans. 42 (1999) 581-591.

[25] J.A. Greenwood, A simplified elliptic model of rough surface contact. Wear 261 (2006) 191-200.

[26] D.J. Whitehouse, Handbook of surface metrology, Institute of physics publishing, Bristol, UK, 1994.

[27] K.J. Stout, E.J. Davis, P.J. Sullivan, Atlas of machined surfaces, Chapman and Hall, London, 1990.

[28] P. Prokopovich, S. Perni, Comparison of JKR- and DMT- Based Multi-asperity Adhesion Model: Theory and Experiment. Coll. Surf. A 383 (2011) 95-101.

[29] K.L. Johnson, J. Greenwood, An approximate JKR theory for elliptical contacts. J. Phys. D Appl. Phys. 38 (2005) 1042-1046.

[30] K.N.G. Fuller, D. Tabor, The effect of surface roughness on the adhesion of elastic solids. Proc. Royal Soc. Series A 345(1642) (1975) 327-342.

[31] X. Tian, B. Bhushan, The Micro-meniscus Effect of a Thin Liquid Film on the Static Friction of Rough Surface Contact. J. Phys. D Appl. Phys. 29 (1996) 163-178.

[32] P. Prokopovich, S. Perni, An Investigation of Microbial Adhesion to Natural and Synthetic Polysaccharide-Based Films and its Relationship with the Surface Energy Components. J. Mater. Sci. Mater. Med. 20 (2009) 195-202.

[33] A. Aka-Any-Grah, K. Bouchemal, A. Koffi, F. Agnely, M. Zhang, M. Djabourov, G. Ponchel, Formulation of mucoadhesive vaginal hydrogels insensitive to dilution with vaginal fluids. Eur. J. Pharmaceutics Biopharmaceutics 76 (2010) 296-303.

[34] K.E. Johnson, Histology and cell biology, Williams and Wilkins Ed., Baltimore, MD, USA. 1991

[35] M. Teodorescu, H. Rahnejat, Dry and wet nanoscale impact dynamics of rough surfaces with or without a self-assembled monolayer. Proc. Instit. Mech. Eng. (J. Nanoeng. Nanosys.- Part N) 221(2) (2007) 49-58.

[36] A.C. Burton, Relation of structure to function of the tissues of the wall of blood vessels. Physiol. Rev. 34(4) (1954) 619-642.

[37] S.P. Jost, J.A. Gosling, J.S. Dixon, The morphology of normal human bladder urothelium. J. Anat. 167 (1989) 103-115.

[38] P.D.H.M. Verhaegen, E.M. Res, A. van Engelen, E. Middelkoop, P.P.M. van Zuijlen, A reliable, non-invasive measurement tool for anisotropy in normal skin and scar tissue. Skin Res. Tech. 16 (2010) 325-331.

[39] S. Korossis, F. Bolland, J. Southgate, E. Ingham, J. Fisher, Regional biomechanical and histological characterisation of the passive porcine urinary bladder: Implications for augmentation and tissue engineering strategies. Biomaterials 30 (2009) 266-275.

[40] P.A. Yuya, E.K. Amborn, M.W. Beatty, J.A. Turner, Evaluating Anisotropic Properties in the Porcine Temporomandibular Joint Disc Using Nanoindentation. Annals Biomed. Eng. 38(7) (2010) 2428-2437.

[41] M.A. Lillie, R.E. Shadwick, J.M. Gosline, Mechanical anisotropy of inflated elastic tissue from the pig aorta. J. Biomech. 43(2010) 2070-2078.

[42] D.P. Sokolis, A passive strain-energy function for elastic and muscular arteries: correlation of material parameters with histological data. Med. Biol. Eng. Comput., 48 (2010) 507-518.

[43] S. Chen, C. Yan, A. Soh, Non-slipping JKR model for transversely isotropic materials Int. J. Sol. Structures 45 (2008) 676–687.

[44] P.R. Nayak, Random process model of rough surfaces in plastic contact. Wear 26 (1973) 305-333.

[45] S. Eichenlaub, G. Kumar, S. Beaudoin, A modeling approach to describe the adhesion of rough, asymmetric particles to surfaces. J. Colloid Interface Sci. 299 (2006) 656-664.

[46] R.P. Jaiswal, G. Kumar, C.M. Kilroy, S.P. Beaudoin, Modeling and Validation of the van der Waals Force During the Adhesion of Nanoscale Objects to Rough Surfaces: A Detailed Description. Langmuir 25(18) (2009) 10612-10623.

[47] G. Carbone, F. Buttiglione, Asperity contact theories: do they predict linearity between contact area and load? J. Mech. Phys. Sol. 56 (2008) 2555-2572.

[48] H. Zahouani, Spectral and 3D motifs identification of anisotropic topographical components. Analysis and filtering of anisotropic patterns by morphological rose approach. Int. J. Mach. Tools Manufact. 38 (1998) 615-623.

[49] P. Prokopovich, S. Perni, R.M. Hall, J. Fisher, Spatial Variation of Wear on Charité Lumbar Discs. Acta Biomater 7 (2011) 3914-3926.

[50] . Yu, A. Polycarpou, A. Contact of rough surfaces with asymmetric distribution of asperity heights. ASME J. Tribol. 124 (2002) 367-376.

[51] N. Yu, A.A. Polycarpou, Combining and Contacting of Two Rough surfaces with Asymmetric Distribution of Asperity Heights. ASME J. Tribol. 126 (2004) 225-232.

[52] J.I. McCool, Non-Gaussian effects in microcontact. Int. J. Mach. Tools Manuf. 32(1) (1992) 115-123.

[53] J.I. McCool, Extending the capability of the Greenwood Williamson microcontact model. ASME J. Tribol. 122 (2000) 496-502.

[54] M. Gotzinger, W. Peukert, Particle adhesion force distributions on rough surfaces. Langmuir 20 (2004) 5298-5303.

Table 1. Contact angles (°) ± S.D. of water (θ_w), ethylene glycol (θ_{et}), hexadecane (θ_h) and surface energy parameters of urethra

θ_w	θ_{et}	θ_h	γ_S^{LW} (mJ/m^2)	γ_S^+ (mJ/m^2)	γ_S^- (mJ/m^2)	γ_S^{AB} (mJ/m^2)	γ_S^{TOT} (mJ/m^2)
57.0± 2.8	49.4 ± 4.0	15.7 ± 1.3	25.39	0.71	29.27	9.12	34.51

Figure captions

Figure 1~~Figure 1~~. Algorithm for the determination of the adhesive force between surfaces based on the multiasperity JKR.

Figure 2~~Figure 2~~. Scheme of the multiasperity adhesion model.

Figure 3~~Figure 3~~**.** (a) 3D example of paraboidal fitting of an asperity and (b) 2D projection with the principal directions.

Figure 4~~Figure 4~~. Asperity height cumulative distribution of urethra.

- data ——— Normal distribution fitting

Figure 5~~Figure 5~~. Frequency of ratio between R_{max} and R_{min} for asperities of urethra.

Figure 6~~Figure 6~~. Cumulative distribution of radii of curvature R_{max} (a) and R_{min} (b) of urethra.

- data ——— Normal distribution fitting ·····Weibull distribution fitting

Figure 7~~Figure 7~~. Simulated profile of contact pressure (a) and area of contact (b) between urethra and PVC.

 Elliptical model presented here ———Approximation using geometrical average of principal radii of curvature

Figure 8~~Figure 8~~. Cumulative distribution of the simulated adhesive pressure.

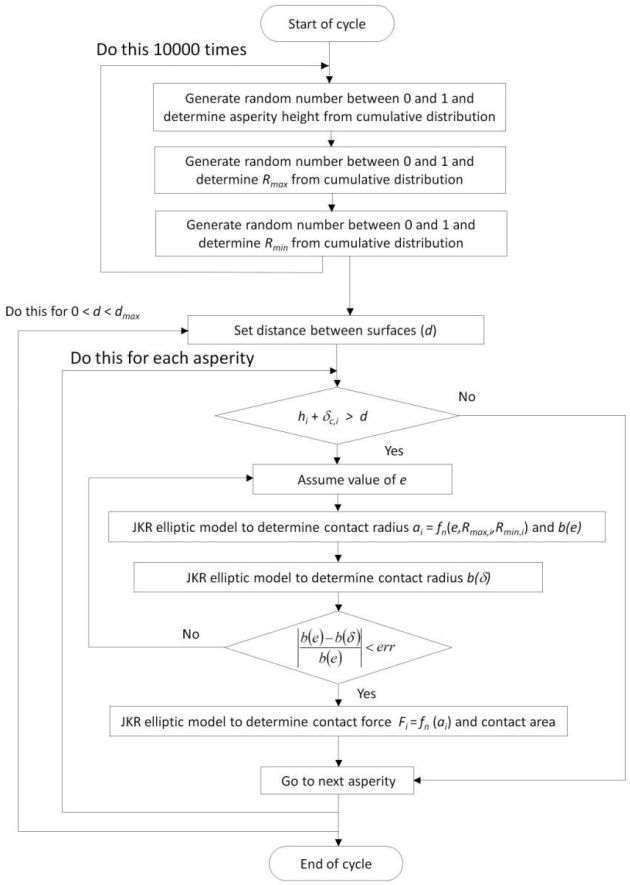
Start of cycle
Do this 10000 times
Generate random number between 0 and 1 and determine asperity height from cumulative distribution
Generate random number between 0 and 1 and determine R_{max} from cumulative distribution
Generate random number between 0 and 1 and determine R_{min} from cumulative distribution
Do this for $0 < d < d_{max}$
Set distance between surfaces (d)
Do this for each asperity
$h_i + \delta_{c,i} > d$
No
Yes
Assume value of e
JKR elliptic model to determine contact radius $a_i = f_n(e, R_{max,i}, R_{min,i})$ and $b(e)$
JKR elliptic model to determine contact radius $b(\delta)$
No
$\left|\frac{b(e)-b(\delta)}{b(e)}\right| < err$
Yes
JKR elliptic model to determine contact force $F_i = f_n(a_i)$ and contact area
Go to next asperity
End of cycle

Figure 1.

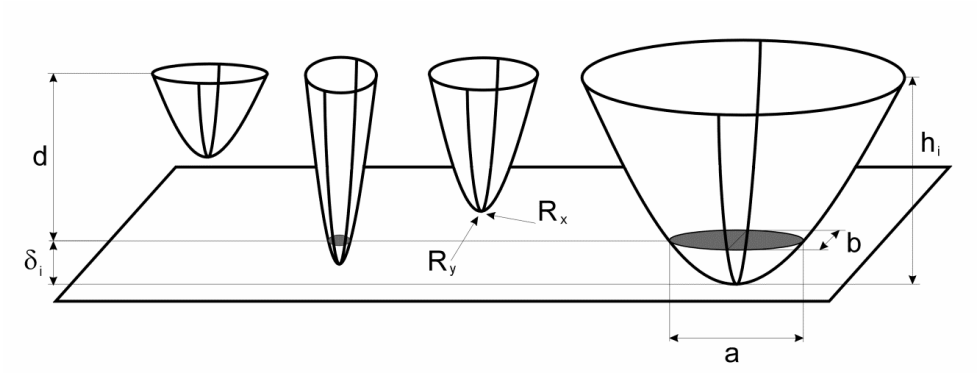

Figure 2.

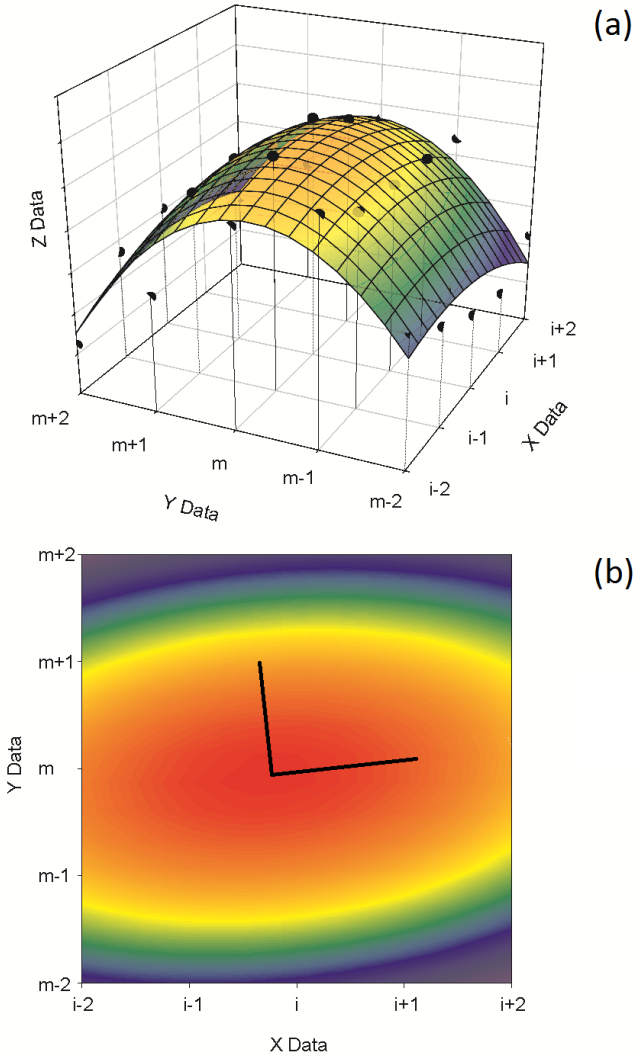
(a)
Z Data
m+2
m+1
m
m-1
m-2
Y Data
i-2
i-1
i
i+1
i+2
X Data
(b)
m+2
m+1
m
m-1
m-2
Y Data
i-2
i-1
i
i+1
i+2
X Data

Figure 3.

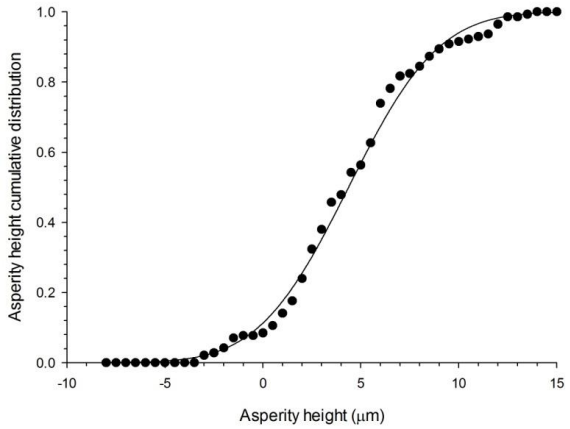
Asperity height cumulative distribution
1.0
0.8
0.6
0.4
0.2
0.0
-10
-5
0
5
10
15
Asperity height (μm)

Figure 4.

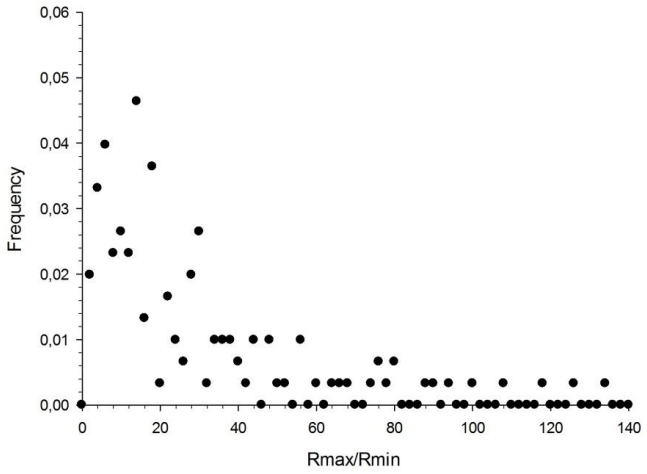
0,06
0,05
0,04
0,03
0,02
0,01
0,00
Frequency
0
20
40
60
80
100
120
140
Rmax/Rmin

Figure 5

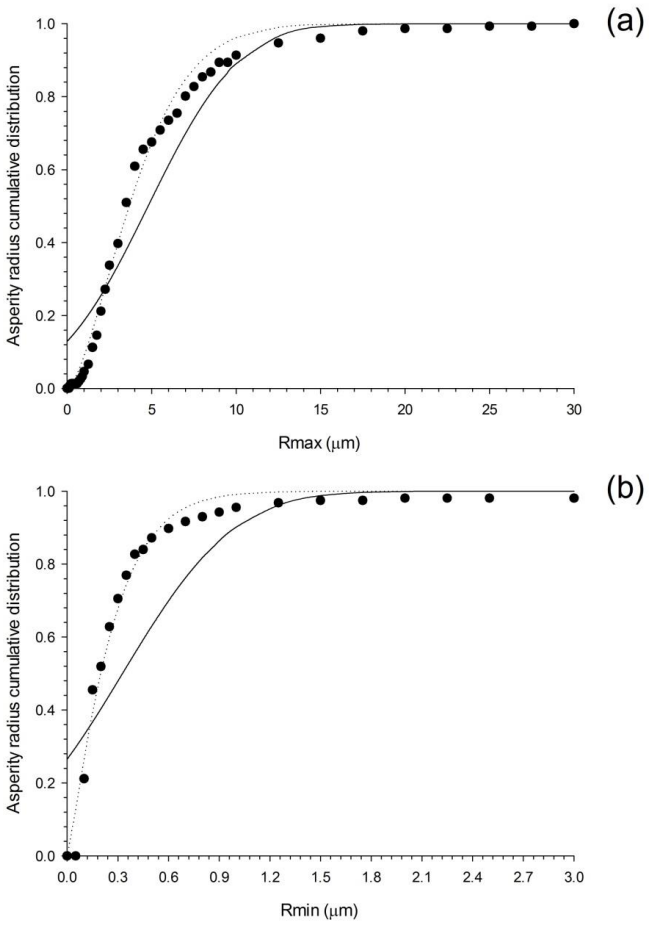
(a)
Asperity radius cumulative distribution
1.0
0.8
0.6
0.4
0.2
0.0
0
5
10
15
20
25
30
Rmax (μm)
(b)
Asperity radius cumulative distribution
1.0
0.8
0.6
0.4
0.2
0.0
0.0
0.3
0.6
0.9
1.2
1.5
1.8
2.1
2.4
2.7
3.0
Rmin (μm)

Figure 6

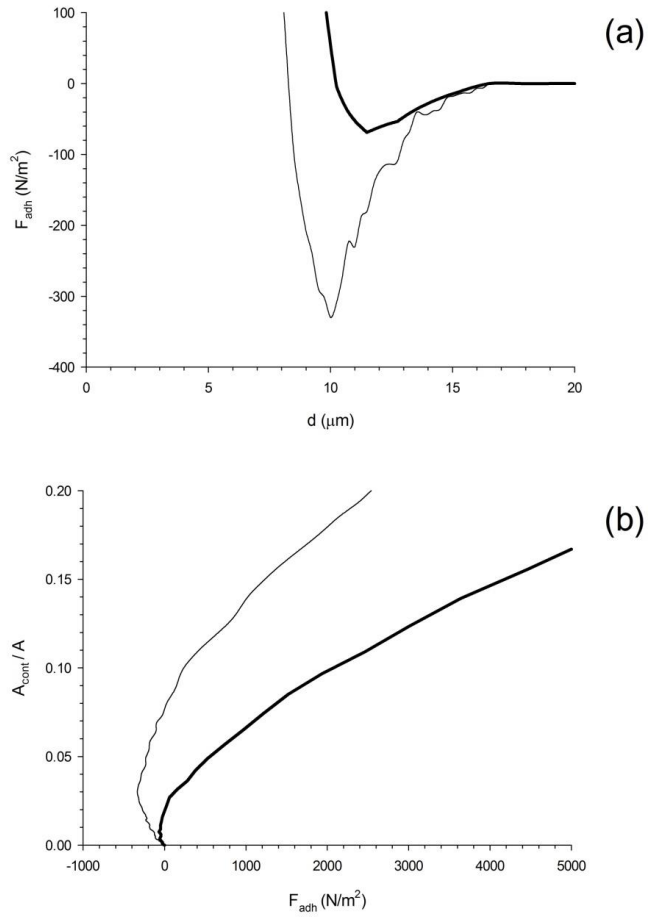
(a)
100
0
-100
-200
-300
-400
F_{adh} (N/m^2)
0
5
10
15
20
d (μm)
(b)
0.20
0.15
0.10
0.05
0.00
A_{cont} / A
-1000
0
1000
2000
3000
4000
5000
F_{adh} (N/m^2)

Figure 7.

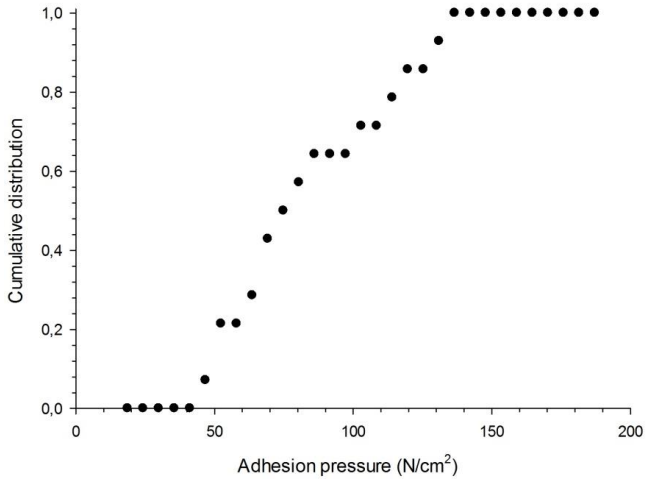
1,0
0,8
0,6
0,4
0,2
0,0
Cumulative distribution
0
50
100
150
200
Adhesion pressure (N/cm2)

Figure 8.